Faraday Discussions

Cite this: *Faraday Discuss.*, 2015, **177**, 345

Probing deactivation pathways of DNA nucleobases by two-dimensional electronic spectroscopy: first principles simulations†

Artur Nenov,*[a] Javier Segarra-Martí,‡[b] Angelo Giussani,‡[b] Irene Conti,[b] Ivan Rivalta,[c] Elise Dumont,[c] Vishal K. Jaiswal,[b] Salvatore Flavio Altavilla,[b] Shaul Mukamel[d] and Marco Garavelli*[bc]

Received 13th September 2014, Accepted 11th November 2014
DOI: 10.1039/c4fd00175c

The SOS//QM/MM [Rivalta *et al.*, *Int. J. Quant. Chem.*, 2014, **114**, 85] method consists of an arsenal of computational tools allowing accurate simulation of one-dimensional (1D) and bi-dimensional (2D) electronic spectra of monomeric and dimeric systems with unprecedented details and accuracy. Prominent features like doubly excited local and excimer states, accessible in multi-photon processes, as well as charge-transfer states arise naturally through the fully quantum-mechanical description of the aggregates. In this contribution the SOS//QM/MM approach is extended to simulate time-resolved 2D spectra that can be used to characterize ultrafast excited state relaxation dynamics with atomistic details. We demonstrate how critical structures on the excited state potential energy surface, obtained through state-of-the-art quantum chemical computations, can be used as snapshots of the excited state relaxation dynamics to generate spectral fingerprints for different de-excitation channels. The approach is based on high-level multi-configurational wavefunction methods combined with non-linear response theory and incorporates the effects of the solvent/environment through hybrid quantum mechanics/molecular mechanics (QM/MM) techniques. Specifically, the protocol makes use of the second-order Perturbation Theory (CASPT2) on top of Complete Active Space Self Consistent Field (CASSCF) strategy to compute the high-lying excited states that can be accessed in different 2D experimental setups. As an

[a]*Dipartimento di Chimica G. Ciamician, Università di Bologna, Via F. Selmi 2, 40126 Bologna, Italy. E-mail: Artur.Nenov@unibo.it; Tel: +39 051 2099495*
[b]*Dipartimento di Chimica G. Ciamician, Università di Bologna, Via F. Selmi 2, 40126 Bologna, Italy*
[c]*Laboratoire de Chimie, Ecole Normale Superieure de Lyon, 46 allée d'Italie, 69364 Lyon, France*
[d]*Department of Chemistry, University of California, Irvine, California 92697-2025, USA*

† Electronic supplementary information (ESI) available: Reference gas-phase calculation of the adenine monomer in gas-phase, adenine π-orbitals, and Cartesian coordinates of all geometries used in this work. See DOI: 10.1039/c4fd00175c

‡ These authors contributed equally to this work.

example, the photophysics of the stacked adenine–adenine dimer in a double-stranded DNA is modeled through 2D near-ultraviolet (NUV) spectroscopy.

1 Introduction

Ultrafast pump–probe spectroscopy experiments backed up by theoretical models at the quantum-mechanical level have achieved a detailed understanding of the photophysics of the DNA building blocks adenine, guanine, thymine and cytosine in gas-phase and solution. A thorough overview of the current status of research is given in several review articles.[1–4] Multimeric nucleobase systems formed through stacking (single-stranded DNA) and base-pairing (double-stranded DNA) add many new facades to the photophysics of single bases: formation and dynamics of exciton states,[5,6] population and decay of intra- and inter-strand charge transfer (CT) states,[7,8] charge separation and recombination,[9–11] ultrafast decay through photoinduced proton transfer,[7,12–15] and formation of lesions.[16–18] Interpretation of the electronic spectra of DNA multimers, which is the entirety of all these processes, is a challenge for the conventional one-dimensional (1D) pump–probe spectroscopy. When multiple electronic transitions come into resonance with the excitation wavelength the spectroscopic signatures of individual de-excitation pathways overlap making their disentanglement virtually impossible. Population transfer between different channels cannot be tracked because the correlation between pump and probe wavelengths is not resolved. This complexity calls for a spectroscopic method with an enhanced spectral resolution. Ultrafast bi-dimensional (2D) spectroscopy holds the premise to disentangle multiple deactivation pathways. First applications in the visible (Vis) and in the near-ultraviolet (NUV) have been documented, resolving energy transfer mechanisms in light harvesting proteins[19,20] and solvation dynamics in nucleotides.[21,22]

The evolution of experimental techniques raises the expectations to theoretical modelling of nonlinear spectra. The theoretical framework of nonlinear electronic spectroscopy has been worked out[23–25] and nowadays methods are sought to feed the resulting equations with system-specific data.[26–28] Static and dynamic studies at the quantum-mechanics level have been successfully applied to study the excited state potential energy surfaces of DNA dimers in gas-phase,[8] in aqueous solution[29] and in the native environment of the solvated single- and double-stranded DNA,[30–32] thus providing a tool for obtaining information about excited state energetics and geometrical deformations. Time-resolved Vis-pump IR/Vis-probe[33] and UV-pump stimulated-Raman-probe[28] spectra simulations demonstrate how quantum-mechanical data can be translated into experimental observables. Simulating ultrafast 2D electronic spectroscopy from first principles is challenging as it requires the incorporation of knowledge about the relaxation dynamics of singly and doubly excited states accessible along the de-excitation pathways into the non-linear spectroscopy simulations. Then, it is the excited state absorption (ESA) and the stimulated emission (SE) whose temporal evolution reflects the geometrical and electronic changes along the potential energy surface. Novel computational and conceptual strategies are required.

The SOS//QM/MM protocol is the first method which couples quantum-mechanics/molecular mechanics (QM/MM) calculations, multi-configurational excited state calculations with non-linear spectroscopy to generate time-resolved

2D electronic spectra.[34] It allows for the characterization of the vertical 1D and 2D electronic spectra of monomeric and dimeric systems with unprecedented details and accuracy.[27,35,36] Prominent features like doubly excited local and excimer states, accessible in multi-photon processes, as well as CT states are revealed. In this paper we present an extension of this protocol to simulate coherent excited state dynamics based on static and dynamic computational data.[37] Under the assumption that the system's time evolution is slow compared to signal generation, we are able to probe single snapshots along the excited state relaxation pathways, which can be achieved experimentally in a pump–probe pulse arrangement through scanning the delay time between the pump and the probe pulse sequences. The protocol is used to generate the spectroscopic signatures at selected geometries along the major deactivation channels of the stacked adenine–adenine (A–A) dimer in an explicitly solvated double-stranded DNA model.

2 Bidimensional time-resolved electronic spectroscopy from first principles

We treat the molecular system as a three-level model, whose eigenstates can be formally divided into: g the ground state; e a set of singly excited states, accessible *via* the pump pulse sequence; and f a set of higher excited states, which are probed after a time delay t_2. The nonlinear response functions for ground state bleaching (GSB), SE and ESA, whose Feynman pathways are shown in Fig. 1 for the rephasing pulse orientation technique, read:[23,24,38]

$$\begin{aligned}
R^{(SOS)}_{\mathbf{k}_1,GSB}(t_1,t_2,t_3) &= -i\hbar^{-3}\Theta(t_1)\Theta(t_2)\Theta(t_3)\sum \boldsymbol{\mu}_{ge}\boldsymbol{\mu}_{eg}\boldsymbol{\mu}_{eg}\boldsymbol{\mu}_{ge} \\
&\quad \times \exp\left[-i\left(\omega_{eg}-i\gamma\right)t_3 - i\left(\omega_{ge}-i\gamma\right)t_1\right] \\
R^{(SOS)}_{\mathbf{k}_1,SE}(t_1,t_2,t_3) &= -i\hbar^{-3}\Theta(t_1)\Theta(t_2)\Theta(t_3)\sum \boldsymbol{\mu}_{g'e'}\boldsymbol{\mu}_{e'g'}\boldsymbol{\mu}_{eg}\boldsymbol{\mu}_{ge} \\
&\quad \times \exp\left[-i\left(\omega_{e'g'}-i\gamma\right)t_3 - i\left(\omega_{ge}-i\gamma\right)t_1\right] \times \mathbb{G}_{e\to e'}(t_2) \\
R^{(SOS)}_{\mathbf{k}_1,ESA}(t_1,t_2,t_3) &= i\hbar^{-3}\Theta(t_1)\Theta(t_2)\Theta(t_3)\sum \boldsymbol{\mu}_{e'f'}\boldsymbol{\mu}_{f'e'}\boldsymbol{\mu}_{eg}\boldsymbol{\mu}_{ge} \\
&\quad \times \exp\left[-i\left(\omega_{fe'}-i\gamma\right)t_3 - i\left(\omega_{ge}-i\gamma\right)t_1\right] \times \mathbb{G}_{e\to e'}(t_2)
\end{aligned} \tag{1}$$

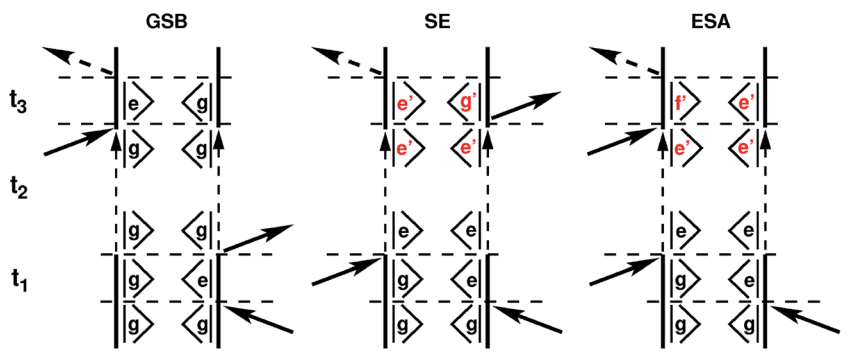

Fig. 1 Feynman diagrams for the rephasing signal including evolution during t_2; GSB = ground state bleaching, SE = stimulated emission, ESA = excited state absorption.

with $\Theta(t)$ the Heavyside step-function, $\boldsymbol{\mu}_{ab}$ the vector of the transition dipole moment between states a and b, ω_{ab} the frequency of the electronic transition between states a and b, γ a phenomenological dephasing rate constant and $\mathbb{G}_{e\rightarrow e'}(t_2)$ a function describing the evolution of the system during the time interval t_2. The transition $e \rightarrow e'$ could describe both evolution in the same electronic state and population transfer to another electronic state. It determines the electronic spectrum of the system after the delay time t_2 which enters eqn (1) through transition frequencies and dipole moments (shown in red). Ideally, quantum or mixed quantum-classical dynamics simulations are conducted to obtain these parameters. Parametrized models which solve the secular Redfield equations have been used to account for population relaxation and Stokes shifts at early times t_2 without explicit dynamics simulations.[39]

The temporal evolution of the nonlinear response is a function of the electronic and geometrical changes in the system modulated by the surroundings. Due to their nature GSB signals do not exhibit time-dependent spectral shifts and their recovery is determined by the decay rates of all excitations resonant with the pump pulse. These features make bleach signals excellent probes for extracting decay rates by means of time-resolved 1D ultrafast spectroscopy. However, the correlation between decay rates and de-excitation pathways cannot be resolved. On the other hand, SE and ESA are specific to each excited state, which makes them eligible probes for pathway-specific extraction of decay rates. Tracking SE and ESA signals by means of 1D ultrafast spectroscopy is challenging as signals from competing channels overlap spectrally and temporally. Furthermore, the temporal evolution of the SE and ESA often span over a large spectral range. 2D time-resolved spectroscopy utilizing broadband probe pulses disentangles spectrally and resolves temporally the fingerprints of the individual de-excitation channels.[40–42]

In this work we employ geometry optimizations in the excited state and probe the higher excited manifold f' and the ground state g' at the obtained stationary points, while keeping the pump pulse pair in resonance with the singly excited state manifold e at the Franck–Condon (FC) point. The local minima are believed to trap excited state population and are, thus, responsible for decay times in the picosecond (ps) time range. With this approach the characteristic spectral signatures of different de-activation channels can be obtained. To compute the fingerprints of each de-excitation channel we regard the channels as independent, *i.e.* we assume that no population is transferred between them or to the ground state (GS) during relaxation from the FC region. With this simplification the 2D spectrum of the FC point can be formally divided along ω_1 into traces resonant with either transition. The time-dependent variation of the traces is analyzed by comparing the signals at the FC point and at the stationary points obtained in this study.

The following approximations are adopted: the system evolves coherently along the populated excited state, *i.e.* inhomogeneous broadening is neglected; coherence dynamics during t_1 and t_3 are neglected, *i.e.* the system's time evolution is assumed to be slow compared to the signal generation; inter-state coherences (*i.e.* the system is not in a population state during t_2 in the SE and ESA diagrams, Fig. 1) are assumed to decay prior to probing. FC active vibrational modes were considered out of the scope of the present work, although several studies on DNA/RNA nucleobases[43–45] report their influence on the photochemical decay path, as

well as on the inherent spectroscopic fingerprints in techniques like electronic circular dichroism.[46,47] To the best of our knowledge simulations considering FC active modes refrain to the use of only a few degrees of freedom considered of importance in the molecule, a strategy that is not always accurate enough to embody the essentials of the molecular system under study.[48] Multidimensional problems could become affordable with recent techniques based in multilayer approaches,[49] making the FC active vibrational modes and its role on the excited state deactivation pathways a whole different avenue of research.

Note that geometry optimizations do not contain temporal information and, therefore, we cannot provide time delays. For simulating quasi-absorptive (rephasing and non-rephasing) 2D electronic spectra we have combined the QM/MM methodology, which provides the transition dipole moments at the Complete Active Space Self Consistent Field (CASSCF) level[50] and transition energies corrected at the second-order Perturbation Theory (CASPT2),[51] with the sum-over-states (SOS) approach.[52] SOS calculations were performed with Spectron 2.7 (ref. 24) readapting the energy levels calculated at each stationary point in order to include the GS bleaching at the FC, *i.e.* by maintaining the FC g–e energy gap and rigidly shifting all the f' energies calculated at the stationary point in order to align the e' energy with the FC e energy.

Using the fingerprint traces and adopting some assumptions supported by experimental data and the mechanistic picture obtained at the *ab initio* computational level ideal 2D spectra for different scenarios can be simulated. These spectra show how static data from excited state optimizations and minimum energy path calculations can be translated into spectroscopic signatures.

3 Application to the adenine–adenine dimer in solvated DNA

3.1 Experimental and theoretical observations for poly-deoxyadenosine systems

Femtosecond (fs) transient absorption experiments by Kohler and co-workers support a model in which DNA multimer excitations decay to long lived exciplex states with a decay time constant ranging from ten to hundreds of ps.[53] Adenine homopolymers and homoduplexes made of adenine–thymine base pairs show much slower decay times compared to those of isolated bases.[1,2,54,55] More recent findings support the fact that long lived excited states decay more rapidly in double-stranded poly-deoxyadenosine–deoxythymine (*i.e.* poly(dA–dT)) than in single stranded poly(dA) sequences,[56,57] addressing the role of inter-strand proton transfer in the deactivation mechanism.[7,12,13] Long-lived signals have also been probed by means of fluorescence up-conversion techniques,[5,58,59] and more recently through femtosecond infrared spectroscopy by probing the distinct cationic and anionic species formed in the process.[10] The experimental findings suggest that excited states localized on just two stacked bases are the common trap states independently of the number of stacked nucleotides.[6,60] On the other hand, Markovitsi and co-workers have postulated the possible delocalization of the exciton over several nucleobases[5,58,59] (up to six according to some theoretical models[61]) by means of fluorescence up-conversion experiments. They suggest that the long-lived component is caused by charge relocalization on the excited

monomers. The de-excitation channels present in systems such as the adenine–thymine base pair have been recently studied with 2D photon echo IR spectroscopy, yielding novel fingerprints that embody the different motions undergone by the molecules during the relaxation process.[62,63]

Several computational works have been undertaken on DNA multimer models to elucidate how light interacts with these electronically and structurally complex systems. Merchán and co-workers computed energies and structure of adenine homodimers in vacuum and in water at CASPT2 level.[8] They support the idea that the long-lived excited states seen in DNA are of CT type, formed by stacking of two bases. Two stacked conformations were characterized, a perfectly stacked "face-to-face" orientation and a poorly stacked orientation where both nucleobases are twisted. Going from the poorly stacked towards the perfectly stacked conformation the CT states decrease in energy, therefore concluding that the population of the CT states upon photoexcitation strongly depends on the conformational properties of DNA. They associate the sub-ps life-time with two parallel routes: one leads to the formation of the excited CT complex, the other to the decay to the ground state directly from L_a state. The formed CT state would display much slower decay times (*i.e.* in the ps regime), as the system has to overcome an energy barrier to access a conical intersection (CI) with the GS. A time-dependent density functional theory (TD-DFT) study by Barone and co-workers concerning different single- and double-stranded poly(dA) multimers embedded in water (treated as a polarizable continuum) also indicate that the long living component of the excited state population correspond to a dark exciplex produced by a charge transfer between stacked adenines.[29] In their study the exciplex constitutes the absolute excited state minimum. A QM/MM study by Plasser *et al.* utilizing the multi-reference configuration interaction (MRCI) *ab initio* method on the adenine dinucleotide in water predicts the formation of several stable low lying exciplexes of $n\pi^*$ and $\pi\pi^*$ character with short inter-molecular separation but without notable charge transfer. The authors suggest that the long life-time results from trapping the system in these minima.[31] Based on QM/MM computations of the adenine monomer and homodimer embedded in a double-stranded DNA, instead, Conti *et al.* propose that an intra-monomer mechanism associated with relaxation of the L_a channel is compatible with the observed multi-exponential decay, including the longer (>100 ps) life-time component.[64,65] Summing up, there is still no agreement on the de-excitation mechanisms in nucleobase multimers, particularly regarding the participation of CT states.

3.2 Mechanistic picture and de-excitation pathways

In the following we outline the recent results of Conti *et al.* for the adenine dimer embedded in a double-stranded DNA model.[65] Both nucleobases were treated quantum-mechanically at CASPT2//CASSCF level with the surrounding DNA chain and solvent represented through point charges. The bright excited states with $L_a(3')$ and $L_a(5')$ character (3′ and 5′ denote the upper and lower nucleobase in the stacked dimer in Fig. 2) couple and form an exciton pair $L_a(3') - L_a(5')/L_a(3') + L_a(5')$ which absorbs around 5.00 eV with a small splitting of 0.05 eV (500 cm^{-1}). After excitation the exciton states evolve toward monomer localized excitations with a deactivation mechanism similar to the one reported in gas-phase, occurring through a C_2 puckering distortion[66–70] (see Fig. 2 $\sim 65^\circ$ at the CI). After the

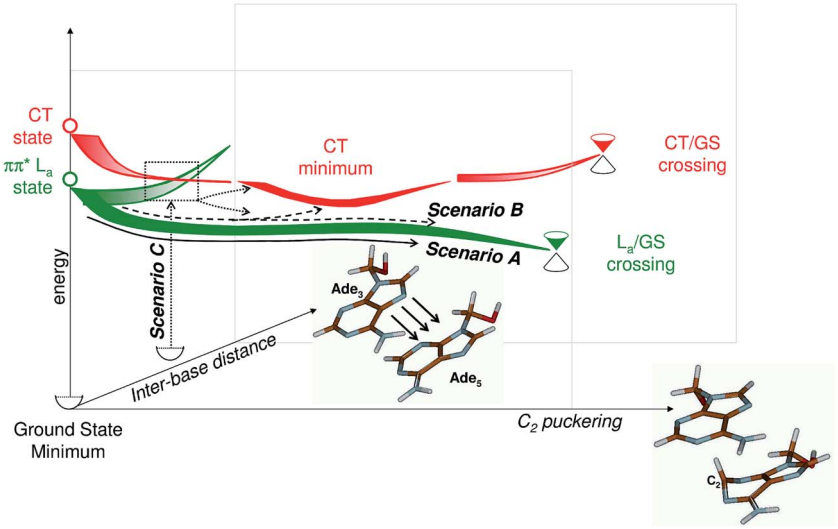

Fig. 2 Schematic representation of the photophysics of the stacked adenine–adenine dimer embedded in a double-stranded DNA in the space of C_2 puckering and inter-base distance following the findings of ref. 65; three hypothetical de-excitation mechanisms are shown: (A) exclusively through locally excited states of L_a character (solid lines); (B) *via* populating the CT states out of the L_a plateau through intra-molecular vibrational energy redistribution (dashed lines); (C) *via* populating both La and CT states directly in the FC region (dotted lines); GS = ground state, CT = charge transfer.

initial energy minimization, associated with bond rearrangements, a broad plateau is reached (Fig. 2). Only at large twisting angles (*i.e.* above 50°) the excited state energy decreases again towards the CI. Conti *et al.* suggest that the lack of a steep gradient towards the CI may be the cause for the long life-time encountered in poly(dA) multimers.

At the relaxed GS geometry the lowest pair of CT states (highest occupied molecular orbital HOMO(3′) → lowest unoccupied molecular orbital LUMO(5′) and HOMO(5′) → LUMO(3′)) are located above 6.00 eV, *i.e.* well above the L_a and L_b bands (Fig. 2).[32] They are found to mix with the energetically close lying bright B_a and B_b bands borrowing partially their oscillator strength. The energetic position of the CT states makes them inaccessible *via* NUV pumping. However, the energetic position of CT states is a dynamical feature modulated by thermal fluctuations which might allow low-lying CT states with energies even in the range of the L_a absorptions.[8,71] Upon optimization the CT character can be traced down to the first excited state where local CT minima are encountered. These minima are characterized through shortening of the inter-base distance of *ca.* 0.6–0.9 Å, accompanied by significant bond rearrangements in both chromophores aiming at stabilizing the charges. Two CI mediated deactivation pathways out of the minima are encountered for each CT state: a proton-transfer and an intra-molecular deformation. Both CIs are accessible only *via* barriers which offer another potential source of the long life-time encountered in poly(dA) multimers.[5,53,58,59,72] We note, however, that the barriers evaluated by Conti *et al.* are too large (∼1 eV) to correlate with ps life-times. Furthermore, despite a thorough search conformations with a CT state below 5.50 eV could not be located.

In the course of geometry optimization Conti *et al.* observe that the C_2 puckering distortion is a common feature of both the L_a and CT relaxation pathways, even though the C_2 puckering along the CT pathway is less pronounced. Along the L_a deactivation pathway the puckering is a result of the ethylene-like twist around the C_2–N_3 double bond, necessary to reach the CI. Along the CT deactivation pathway the puckering reduces the electron repulsion of the excess charge density in the negatively charged monomer. A 2D map in the space of the puckering and inter-base distance coordinates indicates that population transfer through vibrational energy redistribution can occur in both directions *via* small barriers.[65] The oscillation between deactivation channels is likely to slow down the de-excitation process.

3.3 Computational details

The critical geometries obtained in the mechanistic study of the bright exciton states $L_a(3') - L_a(5')$ and $L_a(3') + L_a(5')$ and of the lowest CT states $CT(5' \rightarrow 3')$ and $CT(3' \rightarrow 5')$ are used to generate time domain 2D electronic spectra. For this purpose excited state calculations of the refined GS snapshot and of the excited state minima were performed with Molcas 7.7 (ref. 73) at the state averaged (SA)-CASSCF level including two occupied (HOMO − 1, HOMO, see Fig. S1 in the ESI†) and two virtual (LUMO, LUMO + 1, see Fig. S1 in the ESI†) π-orbitals on each chromophore in the active space (*i.e.* CASSCF(8,8)). Calibration against full active space calculations of the adenine monomer in gas-phase shows that this highly reduced AS does not permit quantitative predictions (details in the ESI†). In fact, a number of transitions accessible by visible light out of the L_a band, which involve lower occupied and higher virtual π-orbitals, are missed. Despite this, the reference calculations demonstrate that doubly excited states which arise *via* excitations among HOMO − 1, HOMO, LUMO and LUMO + 1 acquire the highest oscillator strengths and, thus, dominate the NUV spectral window. We expect these excited states to be affected the most along the de-excitation pathways, considering that they involve the same orbitals as the optimized L_a and CT states. Thus, our efforts focus in resolving the qualitative spectral dynamics of the ESA into the doubly excited states in the NUV spectral window between 20 000 cm^{-1} and 40 000 cm^{-1} from the L_a band (*i.e.* between 60 000 cm^{-1} and 80 000 cm^{-1} from the GS). A shift of 3000 cm^{-1} was applied to all states (implies a 6000 cm^{-1} shift of all mixed doubly excited states) in order to better reproduce the reference calculations. This shift has no effect on the position of the SE and ESA in the spectra, but blue-shifts the GSB by 3000 cm^{-1}. The generally contracted ANO-L basis set was utilized and the following contraction scheme was adopted: C, O/[3s2p1d] and H/[2s].[74] Subsequent energy refinement was done perturbationally with the multi-configurational counterpart of the Møller–Plesset method, denoted as CASPT2, in its single state (SS) version. An imaginary shift of 0.2 (ref. 75) and an ionization potential electron affinity (IPEA) shift of 0.0 (ref. 76) were used. 60 states were included in the state-averaging procedure. The number of roots was chosen to include excitations which upon CASPT2 correction lie in the energy ranges reported in the electronic spectra. Transition dipole moments were calculated at the CASSCF level. The MM part of each snapshot was treated as a set of external point charges in both CASSCF and CASPT2 calculations. The Cholesky decomposition approximation was used to speed up the calculation of two-

electron integrals.[73] A constant dephasing of 250 cm^{-1} was employed with finite transform-limited Gaussian pulse envelopes corresponding to a bandwidth of 10 000 cm^{-1}. While this broadening is unrealistic it serves the purpose of showing the fingerprints of each channel in a broad spectral window, which would provide valuable information for designing experiments with tailored probe pulses. Spectra are plotted on a linear scale.

3.4 Traces for L_a and CT

First, we discuss the traces of the individual excited state relaxation pathways out of the FC region towards the local minima.

We begin with the trace of the L_a de-excitation channel from the FC region to the broad plateau in the relaxed potential energy surface. Due to the flat energy profile the position of the local minimum depends crucially on the computational level used to describe the dynamic correlation. To deal with this issue we selected two representative geometries with C_2 puckering 11° and 40° for generating the spectra. The L_a band gives rise to the most intense transitions in the NUV, absorbing around 39 000 cm^{-1}. They are delocalized over both nucleobases due to exciton coupling forming the exciton states $L_a(3') - L_a(5')$ and $L_a(3') + L_a(5')$. Fig. 3 shows the positive linear combination which collects most of the oscillator strength in the NUV. The region around the GSB of the $L_a(3') + L_a(5')$ (37 000–41 000 cm^{-1}) is congested with off-diagonal bleach signals (*e.g.* peak 2) and ESA to mixed doubly excited states (*e.g.* $L_a(3' + 5')$ peak 5) and is hard to disentangle. Therefore, we encourage the performance of experiments in the low energy window below the bleach region. Pairs of ESA peaks appear (peaks 3|4, and 6|7), which arise *via* probing the local doubly excited states $D_1^*(3'/5')$ and $D_2^*(3'/5')$ out of the L_a band. The ESA doublets 3|4, and 6|7 split as the system leaves the FC region and the exciton localizes on one of the bases. Thereby, the ESA to doubly excited states on the puckered adenine exhibit no blue-shift (peak 3) or red-shifts (peaks 6 and 8) while ESA to doubly excited states on the unmodified adenine exhibit a blue-shift (peaks 4 and 7) equal to the red-shift of the SE (peak 1′). The pronounced red-shift of peaks 6 and 8 indicates that the geometrical

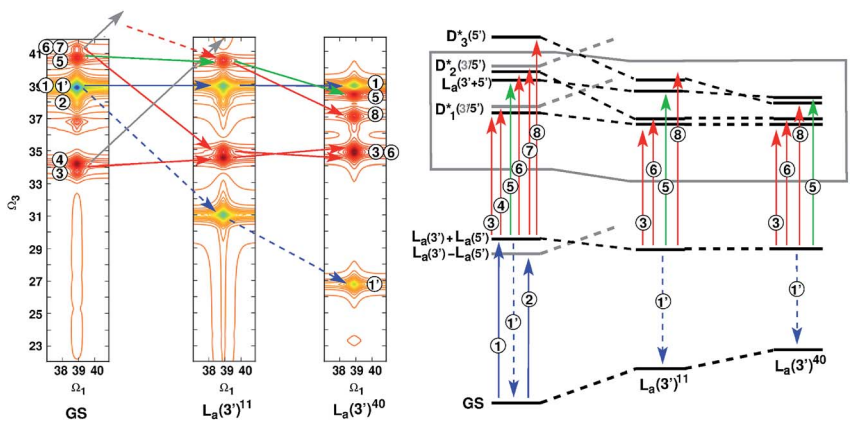

Fig. 3 ESA and SE evolution along the L_a relaxation pathway: (left) spectral traces at critical points; (right) level scheme.

deformations along the L_a relaxation pathway stabilize local doubly excited states even stronger which is a remarkable finding. The SE red-shifts continuously even as the excited state reaches a plateau since the GS exhibits constant destabilization with C_2 puckering deformation.

We note that in a real spectrum the low energy window (*i.e.* below 33 000 cm^{-1}) will exhibit peaks coming from ESA to singly excited states which remain unresolved with the small active space used in this study. Nevertheless, since these states involve orbitals other than HOMO − 1, HOMO, LUMO and LUMO + 1, we expect that their signals will blue-shift along the relaxation pathway. We also note that the absolute positions of the fingerprint ESA are likely to change following more accurate computations. Exemplarily, comparison with reference gas-phase calculations indicates that peak 3 appears around 30 000 cm^{-1}. Nevertheless, our findings make peaks 3, 6 and 8 unique for the L_a relaxation pathway.

In contrast to local excited states, the spectroscopic trace of the CT states is dynamic, depending on the energetic fluctuations of the CT energy levels given by the GS dynamics and on the mixing with degenerate transitions. Our calculations indicate that stabilization down to the NUV region alone is not enough to promote a notable fraction of molecules into the CT states upon NUV pumping, as the oscillator strength of CT states remains generally weak, albeit increasing with respect to unstacked conformations. A noteworthy gain is only possible through mixing with the L_a band. As a consequence, the CT state would inherit oscillator strength and ESA features of the L_a band, whereas the positions of these features would fluctuate with the energy of the CT. In Fig. 4, we focus solely on the spectral characteristics of a pure CT state in order to disentangle in such ideal spectrum its characteristic components that are hard to monitor experimentally, due to the weak oscillator strength of pure CT states. In the relaxed GS geometry the lowest CT state (*i.e.* CT(3′ → 5′)) lies at 6.10 eV with respect to the GS, therefore, pumping occurs with a far-UV (FUV) pulse centered at 49 000 cm^{-1}. Since we are interested in the NUV spectral window, probing is done in the 20 000–40 000 cm^{-1} range, where the diagonal GSB of the CT (peak 3) cannot be resolved. An off-diagonal bleach signal at 38 900 cm^{-1} attributed to the L_a bleaching (peak 1) is visible. In the FC region the spectral window below the L_a bleach is lacking intense ESA,

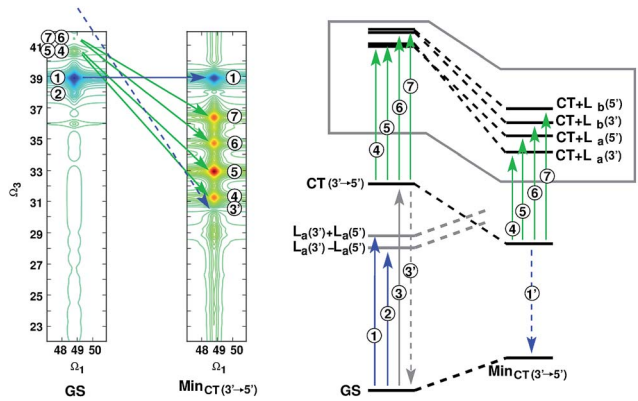

Fig. 4 ESA and SE evolution along the CT relaxation pathway: (left) spectral traces at critical points; (right) level scheme.

whereas four intense peaks appear at the CT minimum. They originate from strongly red-shifted transitions to mixed doubly excited states which, based on wavefunction analysis, we label CT + $L_a(3')$ (peak 4), CT + $L_a(5')$ (peak 5), CT + $L_b(3')$ (peak 6) and CT + $L_b(5')$ (peak 7). Exemplarily, CT + $L_a(3')$ denotes a local HOMO → LUMO excitation in the positively charged moiety of the exciplex. The red-shifted broad ESA feature is the fingerprint of the lowest CT states in the aggregate. The strong red-shift indicates that the L_a/L_b transitions are stabilized along the CT de-excitation pathway in support of the finding that geometrical deformations along these pathways present similarities.

3.5 2DNUV spectra for hypothetical deactivation scenarios

At this point we have enough information to generate ideal 2DNUV ultrafast spectra for various scenarios. Thereby, we make use of the experimental observation that in a poly-adenine DNA single strand the decay times ($\tau_1 = 0.39$ ps, $\tau_2 = 4.3$ ps, $\tau_3 = 182$ ps)[77] differ by an order of magnitude. We assume that leaving the FC region, fast and slow decay do not overlap temporally. Thus, in the ps regime only ESA and SE originating from the deactivation channel responsible for the long life-time survive.

Fig. 5 shows ultrafast 2D spectra for three hypothetical de-excitation mechanisms. Pumping is done with 733 cm^{-1} broad pulses (corresponds to a 20 fs Fourier limited pulse) centered at 38 000 cm^{-1}, while 2932 cm^{-1} broad pulses centered at 34 000 cm^{-1} are used for probing. Plotting is done on a linear scale.

3.5.1 Mechanism A: deactivation exclusively through local excited states. The first hypothetical mechanism (A, Fig. 5 upper panel) that we consider involves the following features:

• Both exciton states $L_a(3')$ + $L_a(5')$ and $L_a(3')$ − $L_a(5')$ are populated upon excitation;

• The CT states are not populated in the FC and do not play a role in the deactivation process;

• the L_a plateau can be reached from each exciton state populated in the FC point through bifurcation of the wavepacket in the femtosecond regime;

• Due to the plateau on the potential energy surface of L_a the wavepacket undergoes spreading in the ps regime.§

According to mechanism A the exciton state $L_a(3')$ + $L_a(5')$, which absorbs at 38 900 cm^{-1} dominates the spectrum, the weaker $L_a(3')$ − $L_a(5')$ state, which absorbs at 38 500 cm^{-1}, introduces asymmetry in the signals. Two ESA bands, one around 33 000–35 000 cm^{-1} and another one around 36 000–37 000 cm^{-1} are observed. On a femtosecond timescale the SE red-shifts to 31 000–32 000 cm^{-1}, the ESA around 33 000–35 000 cm^{-1} blue-shifts by 1000 cm^{-1} and becomes more intense, while the ESA around 36 000–37 000 cm^{-1} disappears. On a ps timescale the SE spreads in the Vis part of the spectrum between 26 000–32 000 cm^{-1} and consequently its intensity decreases. The ESA around 34 000–36 000 cm^{-1} stays compact and retains its intensity. Intuitively, this ESA behavior could be attributed to a compactness of the wavepacket and coherent dynamics in the excited

§ The wavepacket spreading along the L_a is accounted for by averaging the spectra over 10 snapshots generated by interpolating energies and transition dipole moments between $L_a(5')$ (ref. 7) and $L_a(5')$,[40] as well as between $L_a(3')$[11] and $L_a(3')$.[40]

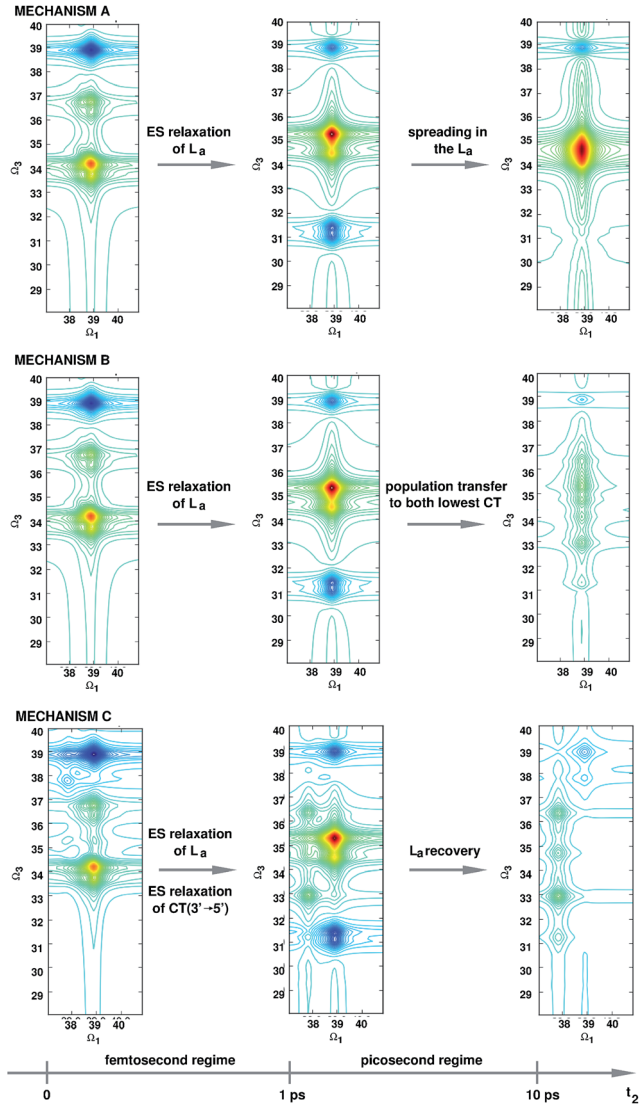

Fig. 5 2DNUV spectra for three hypothetical deactivation mechanisms. The details are given in Sec. 3.5.

state. This behavior reflects the presence of a flat excited state profile along the L_a de-excitation pathway.

3.5.2 Mechanism B: deactivation involving population of CT states through intra-molecular vibrational energy redistribution. The second hypothetical deactivation mechanism (B, Fig. 5 middle panel) involves the following features:

- Both exciton states $L_a(3') + L_a(5')$ and $L_a(3') - L_a(5')$ are populated upon excitation;
- The CT states are not populated in the FC;
- The L_a plateau can be reached from each exciton state populated in the FC point through bifurcation of the wavepacket in the femtosecond regime;

• When reaching the L_a plateau of each base the wavepacket bifurcates again; most of the L_a population decays rapidly (*i.e.* in the few-ps regime) to the GS, while a non negligible fraction is transferred to a CT channel through intra-molecular vibrational energy redistribution where it gets trapped in the corresponding minimum;

• As a result of the observations of Conti *et al.* CT($3' \rightarrow 5'$) is accessible only from the $L_a(5')$ plateau, while CT($5' \rightarrow 3'$) is accessible only from the $L_a(3')$ plateau.

The femtosecond photophysics of the first and second mechanisms are identical. With the majority of L_a population decaying back to the GS in the ps regime the overall spectral intensity decreases. The decay of the L_a population is coded in the partial recovery of the GSB. The population transfer to the CT shows in the broad ESA band between 31 000 cm^{-1} and 37 000 cm^{-1} which emerges along the $L_a(3') - L_a(5')$ and $L_a(3') + L_a(5')$ traces. Computations by Conti *et al.* suggest that mechanisms A and B are correlated, whereby slowing down the relaxation along the flat L_a plateau (mechanism A) facilitates the back-and-forward population transfer between the L_a and CT channels. Provided this mechanism is confirmed experimentally, it is intriguing whether it is a coherent process showing through oscillations between the L_a and CT traces.

3.5.3 Mechanism C: deactivation involving population of CT states in the FC region. The third hypothetical deactivation mechanism (C, Fig. 5 lower panel) involves the following features:

• In 50% of the snapshots the CT($3' \rightarrow 5'$) is stabilized dynamically below the L_a region to ~38 000 cm^{-1} and can be directly populated;¶ note that the percentage and the energetic position of the CT($3' \rightarrow 5'$) state are arbitrary despite some theoretical support;[71]

• The CT($3' \rightarrow 5'$) state mixes with the L_a band in the FC region, borrows oscillator strength and adopts its ESA features;‖

• Local transitions (L_a, $D_1^*(3'/5')$, $D_2^*(3'/5')$ and $D_3^*(5')$) are not affected by the deformations (shortening of the inter-base distance) which stabilize the CT state;

• The L_a plateau can be reached from each exciton state populated in the FC point through bifurcation of the wavepacket in the femtosecond regime;

• The L_a population decays rapidly (*i.e.* in the few-ps regime) to the GS, the CT population is trapped in the local minimum on the excited state.

Although this mechanism is not supported by QM/MM computations,[31,32,65] other groups have considered the possibility to populate low lying CT states directly in the FC region.[8,71] In this regard we would like to draw attention to a recent paper by Rohlfing and co-workers which argues that aqueous solvation may lower CT states by more than 1 eV based on many-body Green's function computations.[71] We believe that only a detailed analysis of the conformational dynamics considering thermal fluctuations instead of analyzing a single representative relaxed geometry will give a definite answer to this pending question.

¶ This is accomplished by red-shifting the energy of the CT($3' \rightarrow 5'$) state, as well as the energies of the mixed doubly excited states CT + $L_a(3')$, CT + $L_a(5')$, CT + $L_b(3')$ and CT + $L_b(5')$ (giving rise to peaks 4–7 in Fig. 4) by 8000 cm^{-1}.

‖ This is accomplished by assigning finite transition dipole moments from the CT($3' \rightarrow 5'$) state to the local doubly excited states accessible from the L_a states ($D_1^*(3'/5')$, $D_2^*(3'/5')$ and $D_3^*(5')$ in Fig. 3).

At the FC point the CT trace appears in the long-wavelength region of the NUV absorption band. Due to mixing with the L_a band L_a features appear as weak ESA along the CT trace at ~35 500 cm^{-1} and ~38 000 cm^{-1}, blue-shifted by 1000 cm^{-1} with respect to the intense ESA along the $L_a(3') + L_a(5')$ trace. In the femtosecond timescale the L_a channel relaxes to its plateau, while the CT channel relaxes to its local minimum $Min_{CT(3' \rightarrow 5')}$ and the CT fingerprints are clearly recognized. In the ps regime only the CT fingerprints survive. The fs population recovery is again coded in the GSB of both the L_a and CT bands. Note, that neither GSB recovers completely as there is still population in the excited state. Comparison between the second and third mechanisms demonstrates the sensitivity of 2D spectroscopy in resolving population transfer (B). Furthermore, 1D pump–probe spectroscopy, in which the 2D spectra collapse along ω_1, will hardly discriminate the ps signatures of these two mechanisms.

4 Conclusion

In this contribution we provided a framework for simulating time-resolved 2D electronic spectroscopy experiments relying on accurate *ab initio* methods. The SOS//QM/MM protocol requires transition energies of singly and doubly excited states together with the transition dipole moments among them. While dynamics simulations are necessary to cover all feasible de-excitation pathways and to collect enough information for simulating non-homogeneous broadenings, already static computations (*i.e.* geometry optimizations, minimum energy path calculations) may provide information on the temporal evolution of individual deactivation channels and may be used to generate ideal 2D spectra in support of hypothetical scenarios, derived from the mechanistic picture. To assess the validity of these ideal spectra a thorough modelling on top of mixed quantum-classical dynamics simulations is required.

The SOS//QM/MM protocol is a hybrid approach and as such it can profit from the progress in three different fields of research: QM/MM dynamics, excited state computations and non-linear spectroscopy. Potential improvements range from employing polarizable force fields[78] or orbital-free embedding[79] to treat the environment in the QM/MM dynamics *via* using more flexible wavefunction-based techniques for computing excited states (*e.g.* generalized active space SCF,[80] the density matrix renormalization group approach,[81] the *n*-electron valence state perturbation theory[82]) to using real pulse shapes and accounting for coherence evolution when computing the nonlinear response of the system.[28]

The adenine–adenine stacked dimer embedded in an explicitly solvated double-stranded DNA model was chosen to demonstrate the application of the protocol in practice. Characteristic points along the first excited state potential energy surface were used to generate time-dependent traces of the local L_a and CT exciplex channels. Subsequently, the 2DNUV spectra were simulated for three de-excitation mechanisms: a deactivation exclusively along the L_a surface (mechanism A), a deactivation involving population of CT states through intra-molecular vibrational energy redistribution (mechanism B) and a deactivation associated with populating both the L_a and the CT states in the FC region. A more detailed study will follow using more characteristic points along the potential energy surface, applying more accurate computational methods (*e.g.* increasing the active space), considering the role of the L_b band, including coherence evolution

and parametrized inhomogeneous broadenings, as well as applying a kinetic model to simulate population transfer along and between deactivation channels.

Acknowledgements

M.G. acknowledges support by the European Research Council Advanced Grant STRATUS (ERC-2011-AdG no. 291198). S.M. gratefully acknowledges the support of the National Institute of Health Grant No. GM-59230 and the National Science Foundation through grant no. CHE-1361516.

References

1 C. T. Middleton, K. D. L. Harpe, C. Su, Y. K. Law, C. E. Crespo-Hernández and B. Kohler, *Annu. Rev. Phys. Chem.*, 2009, **60**, 217–239.
2 C. E. Crespo-Hernández, B. Cohen, P. M. Hare and B. Kohler, *Chem. Rev.*, 2004, **104**, 1977–2020.
3 M. S. de Vries and P. Hobza, *Annu. Rev. Phys. Chem.*, 2007, **58**, 585.
4 K. Kleinermanns, D. Nachtigallova and M. S. de Vries, *Int. Rev. Phys. Chem.*, 2013, **32**, 308.
5 I. Vayá, T. Gustavsson, T. Douki, Y. Berlin and D. Markovitsi, *J. Am. Chem. Soc.*, 2012, **134**, 11366–11368.
6 J. Chen and B. Kohler, *J. Am. Chem. Soc.*, 2014, **136**, 6362–6372.
7 C. E. Crespo-Hernández, B. Cohen and B. Kohler, *Nature*, 2005, **436**, 1141–1144.
8 G. Olaso-González, M. Merchán and L. Serrano-Andrés, *J. Am. Chem. Soc.*, 2009, **131**, 4368–4377.
9 F. D. Lewis, H. Zhu, P. Daublain, K. Sigmund, T. Fiebig, M. Raytchev, Q. Wang and V. Shafirovich, *Photochem. Photobiol. Sci.*, 2008, **7**, 534.
10 D. B. Bucher, B. M. Pilles, T. Carell and W. Zinth, *Proc. Natl. Acad. Sci. U. S. A.*, 2014, **111**, 4369–4374.
11 Y. Zhang, J. Dood, A. A. Beckstead, X.-B. Li, K. V. Nguyen, C. J. Burrows, R. Improta and B. Kohler, *Proc. Natl. Acad. Sci. U. S. A.*, 2014, **111**, 11612.
12 N. K. Schwalb and F. Temps, *J. Am. Chem. Soc.*, 2007, **129**, 9272–9273.
13 N. K. Schwalb and F. Temps, *Science*, 2008, **322**, 243–245.
14 V. Saurí, J. P. Gobbo, J. J. Serrano-Pérez, M. Lundberg, P. B. Coto, L. Serrano-Andrés, A. C. Borin, R. Lindh, M. Merchán and D. Roca-Sanjuán, *J. Chem. Theory Comput.*, 2013, **9**, 481–496.
15 J. P. Gobbo, V. Saurí, D. Roca-Sanjuán, L. Serrano-Andrés, M. Merchán and A. C. Borin, *J. Phys. Chem. B*, 2012, **116**, 4089–4097.
16 R. P. Sinha and D.-P. Häder, *Photochem. Photobiol. Sci.*, 2002, **1**, 225.
17 M. Hada and A. G. Georgakilas, *J. Radiat. Res.*, 2008, **49**, 203.
18 A. C. Kneuttinger, G. Kashiwazaki, S. Prill, K. Heil, M. Müller and T. Carell, *Photochem. Photobiol.*, 2014, **90**, 1.
19 E. Collini, C. Y. Wong, K. E. Wilk, P. M. G. Curmi, P. Brumer and G. D. Scholes, *Nature*, 2010, **463**, 644.
20 T. Brixner, J. Stenger, H. M. Vaswani, M. Cho, R. E. Blankenship and G. R. Fleming, *Nature*, 2005, **434**, 625.
21 C. H. Tseng, S. Matsika and T. C. Weinacht, *Opt. Express*, 2009, **17**, 18788–18793.

22 B. A. West and A. M. Moran, *J. Phys. Chem. Lett.*, 2012, **3**, 2575–2581.
23 S. Mukamel, *Principles of Nonlinear Optics and Spectroscopy*, Oxford Unversity Press, Oxford, UK, 1995.
24 D. Abramavicius, B. Palmieri, D. V. Voronine, F. Sanda and S. Mukamel, *Chem. Rev.*, 2009, **109**, 2350–2408.
25 M. Cho, *Two-Dimensional Optical Spectroscopy*, CRC Press, Boca Raton, Florida, USA, 2009.
26 J. Jiang and S. Mukamel, *Phys. Chem. Chem. Phys.*, 2011, **13**, 2394.
27 A. Nenov, I. Rivalta, G. Cerullo, S. Mukamel and M. Garavelli, *J. Phys. Chem. Lett.*, 2014, **5**, 767.
28 B. P. Fingerhut, K. E. Dorfman and S. Mukamel, *J. Chem. Theory Comput.*, 2014, **10**, 1172.
29 F. Santoro, V. Barone and R. Improta, *Proc. Natl. Acad. Sci. U. S. A.*, 2007, **104**, 9931–9936.
30 R. Improta and V. Barone, *Angew. Chem., Int. Ed.*, 2011, **50**, 12016.
31 F. Plasser and H. Lischka, *Photochem. Photobiol. Sci.*, 2013, **12**, 1440.
32 V. A. Spata and S. Matsika, *J. Phys. Chem. A*, 2014, **118**, 12021.
33 D. Polli, P. Altoe, O. Weingart, K. M. Spillane, C. Manzoni, D. Brida, G. Tomasello, G. Orlandi, P. Kukura, R. A. Mathies, M. Garavelli and G. Cerullo, *Nature*, 2010, **467**, 441.
34 I. Rivalta, A. Nenov, G. Cerullo, S. Mukamel and M. Garavelli, *Int. J. Quantum Chem.*, 2014, **114**, 85–93.
35 A. Nenov, I. Rivalta, G. S. Mukamel and M. Garavelli, *Comput. Theor. Chem.*, 2014, **1040**, 295.
36 A. Nenov, S. a. Beccara, I. Rivalta, G. Cerullo, S. Mukamel and M. Garavelli, *ChemPhysChem*, 2014, **15**, 3282.
37 I. Rivalta, A. Nenov, O. Weingart, G. Cerullo, G. S. Mukamel and M. Garavelli, *J. Phys. Chem. B*, 2014, **118**, 8396.
38 P. Hamm and M. Zanni, *Concepts and Methods of 2D Infrared Spectroscopy*, Cambridge Unversity Press, Cambridge, UK, 2011.
39 D. Abramavicius, L. Valkunas and S. Mukamel, *Europhys. Lett.*, 2007, **80**, 17005.
40 G. Aubock, C. Consani, F. van Mourik and M. Chergui, *Opt. Lett.*, 2012, **37**, 2337.
41 N. Krebs, I. Pugliesi, J. Hauer and E. Riedle, *New J. Phys.*, 2014, **15**, 085016.
42 R. B. Varillas, A. Candeo, D. Viola, M. Garavelli, S. D. Silvestri, G. Cerullo and C. Manzoni, *Opt. Lett.*, 2014, **39**, 3849.
43 D. Picconi, V. Barone, A. Lami, F. Santoro and R. Improta, *ChemPhysChem*, 2011, **12**, 1957.
44 D. Picconi, A. Lami and F. Santoro, *J. Chem. Phys.*, 2012, **136**, 244104.
45 D. Picconi, F. J. A. Ferrer, R. Improta, A. Lami and F. Santoro, *Faraday Discuss.*, 2013, **163**, 223.
46 G. Pescitelli, V. Barone, L. D. Bari, A. Rizzo and F. Santoro, *J. Org. Chem.*, 2013, **78**, 7398.
47 D. Padula, D. Picconi, A. Lami, G. Pescitelli and F. Santoro, *J. Phys. Chem. A*, 2013, **117**, 3355.
48 R. Borrelli, M. Thoss, H. Wang and W. Domcke, *Mol. Phys.*, 2012, **110**, 751.
49 H. Wang and M. Thoss, *J. Chem. Phys.*, 2003, **119**, 1289.
50 B. O. Roos, *Ab Initio Methods in Quantum Chemistry: Part II*, Wiley, Chicester, UK, 1987.

51 K. Andersson, P. A. Malmqvist, B. O. Roos, A. J. Sadlej and K. Wolinski, *J. Phys. Chem.*, 1990, **94**, 5483–5488.
52 G. H. Chen, S. Mukamel, D. Beljonne and J. L. Bredas, *J. Chem. Phys.*, 1996, **104**, 5406–5414.
53 T. Takaya, C. Su, K. D. L. Harpe, C. E. Crespo-Hernández and B. Kohler, *Proc. Natl. Acad. Sci. U. S. A.*, 2008, **105**, 10285–10290.
54 C. E. Crespo-Hernández, K. D. L. Harpe and B. Kohler, *J. Am. Chem. Soc.*, 2008, **130**, 10844–10845.
55 K. D. L. Harpe, C. E. Crespo-Hernández and B. Kohler, *J. Am. Chem. Soc.*, 2009, **131**, 17557–17559.
56 K. D. L. Harpe and B. Kohler, *J. Phys. Chem. Lett.*, 2011, **2**, 133–138.
57 B. Kohler, *J. Phys. Chem. Lett.*, 2010, **1**, 2047–2053.
58 I. Vayá, T. Gustavsson, F.-A. Miannay, T. Douki and D. Markovitsi, *J. Am. Chem. Soc.*, 2010, **132**, 11834–11835.
59 I. Vayá, F.-A. Miannay, T. Gustavsson and D. Markovitsi, *ChemPhysChem*, 2010, **11**, 987–989.
60 J. Chen, A. K. Thazhathveetil, F. D. Lewis and B. Kohler, *J. Am. Chem. Soc.*, 2013, **135**, 10290–10293.
61 I. Bucharov, Q. Wang, M. Raytchev, A. Trifonov and T. Fiebig, *Proc. Natl. Acad. Sci. U. S. A.*, 2007, **104**, 4794–4797.
62 C. Greve, N. K. Preketes, R. Costard, B. Koeppe, H. Fidder, E. T. J. Nibbering, F. Temps, I. Andricioaei, S. Mukamel and T. Elsaesser, *J. Phys. Chem. A*, 2012, **116**, 7636–7644.
63 C. Greve, N. K. Preketes, H. Fidder, R. Costard, B. Koeppe, I. A. Heisler, S. Mukamel, F. Temps, E. T. J. Nibbering and T. Elsaesser, *J. Phys. Chem. A*, 2013, **117**, 594–606.
64 I. Conti, P. Altoè, M. Stenta, M. Garavelli and G. Orlandi, *Phys. Chem. Chem. Phys.*, 2010, **12**, 5016–5023.
65 I. Conti, A. Nenov, S. Höfinger, S. F. Altavilla, I. Rivalta, E. Dumont, G. Orlandi and M. Garavelli, *Phys. Chem. Chem. Phys.*, 2015, DOI: 10.1039/C4CP05546B.
66 L. Serrano-Andrés, M. Merchán and A. C. Borin, *Proc. Natl. Acad. Sci. U. S. A.*, 2006, **103**, 8691–8696.
67 L. Serrano-Andrés, M. Merchán and A. C. Borin, *Chem.–Eur. J.*, 2006, **12**, 6559–6571.
68 M. Merchán, R. González-Luque, T. Climent, L. Serrano-Andrés, E. Rodríguez, M. Reguero and D. Peláez, *J. Phys. Chem. B*, 2006, **110**, 26471–26476.
69 A. Giussani, J. Segarra-Mart, D. Roca-Sanjun and M. Merchn, *Excitation of Nucleobases from a Computational Perspective I: Reaction Paths*, Springer, Berlin Heidelberg, 2013, pp. 1–41.
70 I. Conti, M. Garavelli and G. Orlandi, *J. Am. Chem. Soc.*, 2009, **131**, 16108–16118.
71 H. Yin, Y. Ma, J. Mu, C. Liu and M. Rohlfing, *Phys. Rev. Lett.*, 2014, **112**, 228301.
72 C. Su, C. T. Middleton and B. Kohler, *J. Phys. Chem. B*, 2012, **116**, 10266–10274.
73 F. Aquilante, L. De Vico, N. Ferre, G. Ghigo, P. A. Malmqvist, P. Neograd y, T. B. Pedersen, M. Pitonak, M. Reiher, B. O. Roos, L. Serrano-Andres, M. Urban, V. Veryazov and R. Lindh, *J. Comput. Chem.*, 2010, **31**, 224–247.
74 P. O. Widmark, P. A. Malmqvist and B. O. Roos, *Theor. Chim. Acta*, 1990, **77**, 291–306.
75 N. Forsberg and P. A. Malmqvist, *Chem. Phys. Lett.*, 1997, **274**, 196–204.

76 G. Ghigo, B. O. Roos and P. A. Malmqvist, *Chem. Phys. Lett.*, 2004, **396**, 142–149.
77 W.-M. Kwok, C. Ma and D. L. Phillips, *J. Am. Chem. Soc.*, 2006, **128**, 11894.
78 Y. Shi, Z. Xia, J. Zhang, R. Best, C. Wu, J. W. Ponder and P. Ren, *J. Chem. Theory Comput.*, 2013, **9**, 4046.
79 T. A. Wesolowski, *Computational Chemistry: Reviews of Current Trends*, World Scientific, 10th edn, 2006.
80 D. Ma, G. L. Manni and L. Gagliardi, *J. Chem. Phys.*, 2011, **135**, 044128.
81 Y. Kurashige and T. Yanai, *J. Chem. Phys.*, 2011, **135**, 094104.
82 C. Angeli, M. Pastore and R. Cimiraglia, *Theor. Chem. Acc.*, 2007, **117**, 743.

